Energy 109 (2016) 791–802

Contents lists available at ScienceDirect

Energy

journal homepage: www.elsevier.com/locate/energy

Thermodynamic analysis and multi-objective optimization of various ORC (organic Rankine cycle) configurations using zeotropic mixtures

Mohsen Sadeghi, Arash Nemati, Alireza ghavimi, Mortaza Yari*

Faculty of Mechanical Engineering, University of Tabriz, Tabriz, Iran

ARTICLE INFO

Article history:
Received 16 February 2016
Received in revised form
6 April 2016
Accepted 9 May 2016

Keywords:
ORC (organic Rankine cycle)
Zeotropic mixtures
STORC (series two-stage ORC)
Geothermal water
Multi-objective optimization

ABSTRACT

In this paper, the performance of the ORC (organic Rankine cycle) powered by geothermal water, in three different configurations, including the simple ORC, PTORC (parallel two-stage ORC) and STORC (series two-stage ORC), using zeotrpoic working fluids is investigated from the viewpoints of the energy and exergy. In addition, considering the net power output and TSP (turbine size parameter) as the two objective functions, the multi-objective optimization with the aim of maximizing the first function and minimizing the second one, is performed to determine the optimal values of decision variables including evaporators 1 and 2 pressure, the pinch point temperature difference and the superheating degree. The results show that using zeotropic mixtures as the working fluid instead of a pure fluid such as R245fa, leads to 27.76%, 24.98% and 24.79% improvement in power generation in the simple ORC, PTORC and STORC, respectively and also lower values of TSP.

Moreover, it is observed that STORC has the highest amount of net power output and R407A can be selected as the most appropriate working fluid. The optimization results demonstrate that at the final optimum point achieved by Pareto frontier, the values of the objective functions are gained 877 kW and 0.08218 m, respectively.

1. Introduction

General population growth with economic development causes escalating energy consumption [1]. Global warming, rupturing of the ozone layer and other environmental problems lead to the energy policy consideration. In addition, increasing the electricity price up to a rate of 12% annually motivates the use of waste heat and renewable sources for power generation [2,3]. Possible solutions may be the use of ORC (organic Rankine cycle), KC (Kalina cycle) and other types of the low grade heat power generations. Among the proposed cycles, ORCs are considered as a practical solution because of their simplicity, reliability, and flexibility [4]. Geothermal energy, solar energy, ocean thermal energy and waste heat can be used as heat resources for ORC. Geothermal energy is a low-grade heat source that many researches have been done on these criteria recently.

One of the main problems in ORC based power plants is high exergy destruction in these cycles. Based on Venkatarathnam et al. [5] research, the main source of exergy destruction in ORC is evaporator because of the temperature mismatching between the source and the working fluid as shown in Fig. 1. According to this figure which illustrates the heat transfer process between the working fluid and the thermal source in a HRVG (heat recovery vapor generator), the thermal energy transmission to the working fluid occurs at three steps including preheating, evaporating and superheating. As it is obvious from Fig. 1, the temperature remains constant in the evaporating stage in pure fluids leading to a significant temperature difference between the source and the working fluid especially in the higher values of quality which causes more amount of exergy destruction.

In order to minimize this temperature mismatching and reduce the exergy destruction in the cycle, which leads to efficiency rising, numerous studies have been carried out. There are two main possible solutions which are proposed by researchers up to now, including using the zeotropic mixtures and enhancement of cycle configuration.

A zeotropic mixture is a chemical mixture which is combination of different pure fluids. Zeotropic mixtures have a non-isothermal phase change and they never have the same vapor phase and liquid phase composition at the vapor–liquid equilibrium state.

* Corresponding author. Tel.: +98 41 33392477.
E-mail address: myari@tabrizu.ac.ir (M. Yari).

http://dx.doi.org/10.1016/j.energy.2016.05.022
0360-5442/

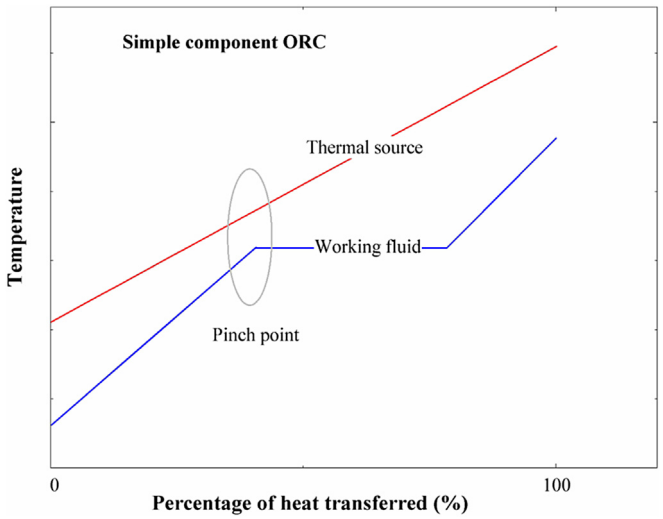

Fig. 1. Temperature mismatching during the heat addition process for a simple component ORC.

Using zeotropic mixtures as a working fluid in the power cycles leads to a temperature variation of the working fluid during the phase change process and causes an improvement of the temperature matching in the evaporator; which is depicted in Fig. 2. By applying this method, the irreversibilities during the vaporization process decreases.

The effects of 10 groups of mixtures on the performance of ORC were analyzed by Kange et al. [6]. The results showed that R245fa/R600a (0.9/0.1) was the most preferable mixture among the working fluids within the scope of this research. Radulovic et al. [7] proposed six zeotropic mixtures for ORC powered by low temperature geothermal heat source. The maximum exergetic efficiency of 47% was achieved by R-143a (0.7)/R-124 (0.3). A comparative analysis between the zeotropic mixtures and R-143a shows that the cycle efficiency can be improved up to 15% at the same operating conditions. Liu et al. [8] studied R600a/R601a mixtures for various mole fractions and proved that the ORC power can be optimized by using this mixture till 11%, 7% and 4% compared to R600a at geothermal water temperatures of 110, 130 and 150 °C, respectively. Yue et al. [9] investigated the performance of a geothermal ORC system using zeotropic working fluids. They concluded that with

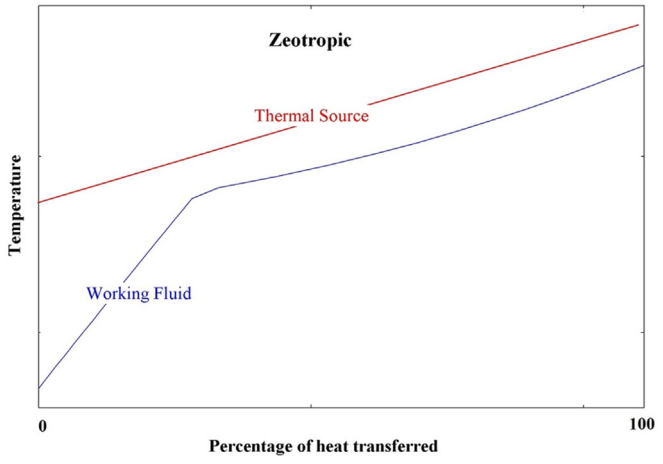

Fig. 2. Improvement of the temperature mismatching during heat addition process for zeotropic mixtures.

use of zeotropic mixtures as the working fluid, the energy and exergy efficiencies increases. Furthermore the results showed that an optimal thermal performance for a certain mole fraction of isopentane in the mixture can be achieved. The thermodynamic analysis of a regenerative ORC with different compositions of R245fa and R152a as the zeotropic working fluid was performed by Deethayat et al. [10]. The results indicated that decreasing the R245fa ratio leads to the reduction of the irreversibilities at the evaporator and condenser. Also, they found that for the mass fraction of R245fa below 80%, the irreversibilities were nearly steady.

S. Lecompte et al. [11] studied the thermodynamic performance of a non-superheated subcritical ORC with zeotropic mixtures as the working fluid from the viewpoint of the exergy. They found that the exergy efficiency increases 7.1%–14.2% compared to the same systems using the pure working fluids. Utilization of the zeotropic mixtures in ORC for waste heat recovery from an industrial boiler is presented by You-Rong Li et al. [12]. They found that comparing the ORC with pure working fluids, the performance of the ORC with zeotropic mixtures is economically improved. Muhsen Habka et al. [13] investigated the potential of organic Rankine cycles using zeotropic mixtures for utilizing the geothermal water. They evaluated the performance of the ORC system with zeotrpic mixtures such as R422A, R22M, R407A and R22D from the viewpoint of the first and second laws of thermodynamics. They reported that R22M and R422A show better performance than the other working fluids in the parallel ORC–CHP system. Heberle et al. [14] studied the exergy efficiency of an ORC using zeotropic mixtures of isobutane–isopentane and R227ea– R245fa as working fluids. They found that compared to the same cycle using pure working fluids, for temperatures lower than 120 °C the second law efficiency increases up to 15%. Moreover, the results showed that the lower mismatching between the working fluid and cooling water temperatures leads to the higher second law efficiency.

Some of the most important investigations for improvement of the cycle configurations are mentioned here. Yari [15] investigated the performance of the various organic Rankine cycles using dry working fluids from the viewpoints of the first and second laws of thermodynamics. The results showed that the energy and exergy efficiency values of the regenerative ORC with an internal heat exchanger is on average 30% more than the simple one. The comparison of a simple ORC, an ORC with an IHE (internal heat exchanger), a regenerative ORC, and a regenerative ORC with an IHE from the energy and exergy point of views was performed by yari [16]. The results demonstrated that the highest amount of the first law efficiency was around 7.65% belonging to the ORC with an IHE and using R123 as the working fluid. Ho et al. [17] investigated several configurations of the OFC (organic flash cycle) in order to power generation enhancement. It is observed that splitting the expansion process into two steps leads to utilization efficiency enhancement around 10% compared to the optimized basic ORC. Exergetic study of a dual-level binary geothermal plant was executed by Kanoglu [18]. As a comparison the results showed that the defined thermal efficiencies of the proposed systems were found 5.8% and 8.9%, respectively. Zhang et al. [19] analyzed a novel system of a dual loop bottoming ORC for waste heat recovery from a diesel engine. They concluded that using the low temperature loop leads to more net power output than that of the high temperature loop. Also, it was shown that in the low load areas, the maximum thermal efficiency can be improved up to nearly 13.15%. Yari et al. [20] studied and compared the performance of three different cycles including: TLC (trilateral Rankine cycle), ORC (organic Rankine cycle) and KC (Kalina cycle) using a low grade heat source from the viewpoint of exergoeconomic. The results indicated that the net power output gained by the TLC system could be greater than that

of the ORC and/or KCS11 systems. Li et al. [21] represented a novel system to decrease the exergy destruction in the evaporator. They implemented two evaporators for this aim and compared the results with those of simple ORC. They concluded that thermal efficiency increases and exergy destruction decreases with this new configuration. They also proposed a new configuration with two evaporators (STORC) in Ref. [22]. They compared this new configuration (STORC) with the previous one (PTORC) and they found that STORC has higher net power and presents excellent systematic performance.

To the best of the author's knowledge and by surveying the mentioned literatures, thermodynamic analysis and multi-objective optimization for various configurations of organic Rankine cycle power generation using zeotropic mixtures are not performed. In order to cover the shortcomings existing in the literature, as a first step, the performance of three different configurations of organic Rankine cycle power generation, including the simple ORC, PTORC and STORC, using zeotropic mixtures as the working fluid are modeled and compared. At the second step, the best configuration and the most suitable working fluid are chosen from the viewpoint of the power generation. Finally, to identify the optimal values of the design parameters for the selected system, the multi-objective optimization using genetic algorithm is carried out. Four key parameters including the evaporator 1 pressure, evaporator 2 pressure, pinch point temperature difference and superheating degree are considered as decision variables and the net power output and the turbine size parameter are the two objective functions.

2. System description and modeling

2.1. System description

Fig. 3 shows the schematic and T-s diagrams of the simple ORC as well as two-stage evaporation ORC systems in two different configurations: PTORC (parallel two-stage organic Rankine cycle) and STORC (series two-stage organic Rankine cycle). The geothermal heat source divided in two temperature ranges that first flows through evaporator 1 and then through evaporator 2. Geothermal hot stream is shown by the red lines; cooling water which is used for condenser cooling is shown by the blue lines and the working fluid of ORC systems are shown via the yellow lines. The heat source and heat sink for the simple ORC, PTORC and STORC are considered exactly the same.

In the simple ORC system, the saturated liquid exiting the condenser is pressurized by the pump to the evaporator where absorbs thermal energy from the geothermal water. Then the superheated vapor at the evaporator outlet goes through the turbine where its pressure drops to the condenser pressure and generates the mechanical work.

In the PTORC configuration the saturated liquid at the condenser outlet is divided into two parts, which is pressurized by pump 1 to a higher pressure level that absorbs heat in evaporator 1 and to a lower pressure which absorbs geothermal water heat in evaporator 2. The outlet vapors from evaporators flow into turbine where their enthalpies are converted into the mechanical energy to drive the generator. The discharging steam from the turbine outlet is led to the condenser where it is liquefied by the cooling water.

In STORC unlike the PTORC the high and low stages are connected to each other in evaporator 2. Besides this difference, STORC and PTORC are almost the same. The saturated liquid working fluid from the condenser outlet first pressurized by pump 2 to a lower pressure level, which flows into the evaporator 2 to absorb heat from geothermal water coming from the evaporator 1. One part of evaporator 2 outlet is saturated liquid which led to pump 1 to pressurized to higher level of pressure (state 3) and other part is superheated vapor that flows through turbine (state 6) [22].

In the present study, ten zeotropic mixtures as well as one pure refrigerant are selected as working fluids. Selection of the zeotropic mixtures is performed by considering safety and environmental properties assessment such as ODP (ozone depletion potential), GWP (global warming potential). Moreover, according to thermal source temperature amount and considering the evaporator pressure as 0.9 P_c, there are two restrictions for selecting of the working

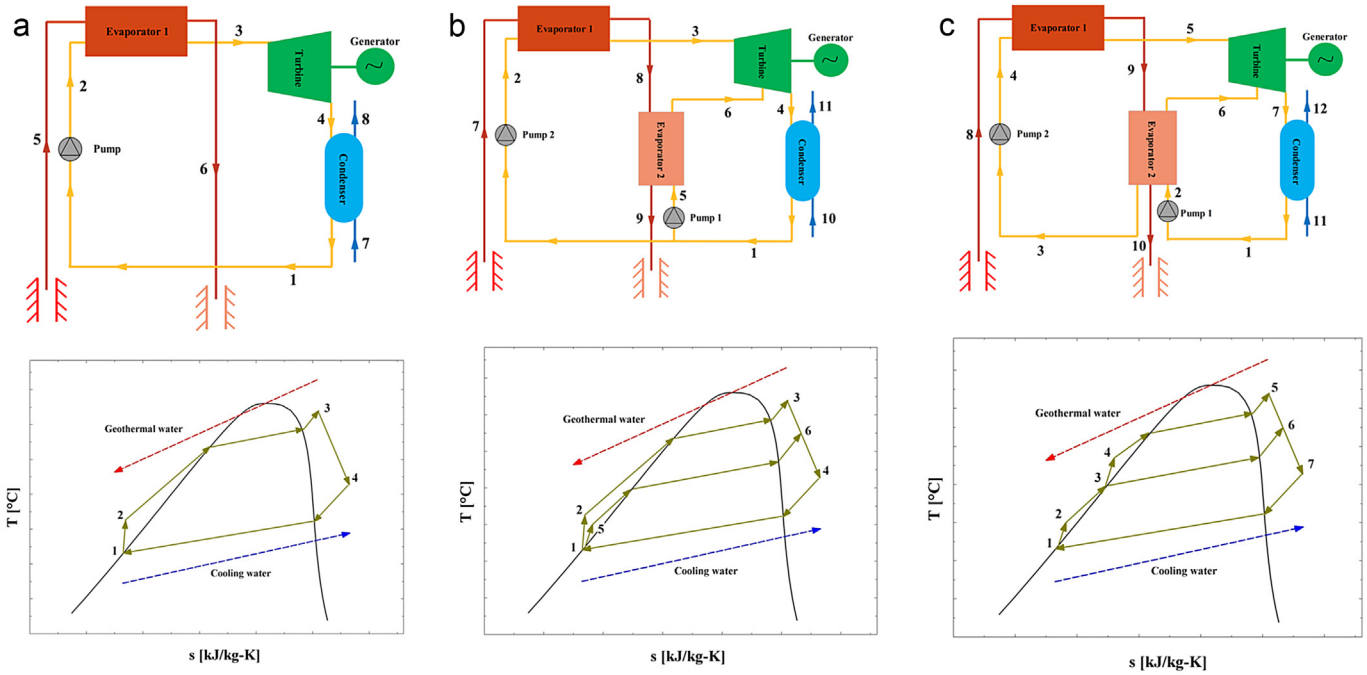

Fig. 3. a) Schematic and T-s diagrams of the simple ORC system. b) Schematic and T-s diagrams of the PTORC system. c) Schematic and T-s diagrams of the STORC system.

fluids: the first one is that the working fluid temperature at 0.9 P_c should not be higher than the source temperature at the pinch point and the second one is avoiding a large temperature difference between the thermal reservoir and the working fluid. The specifications of the recommended fluids are listed in Table 1.

2.2. Assumptions

For modeling and simulating the simple ORC, PTORC and STORC, the following hypotheses are adopted for simplifying the study:

- All cycles operate in a steady state condition.
- All heat exchangers are adiabatic components.
- HRVGs (heat recovery vapor generators) outlets are superheated vapor and saturated liquid is supposed to be condenser outlet.
- Pressure drop in HRVGs and pipelines could be neglected.
- Frictional losses in the mixing process of the high and low pressure vapors in turbine are negligible.
- Performances of the external cycles such as the geothermal water pumps and the cooling water circulation pumps of the condenser are not taken into account, because the geothermal water pumps are independent from the working fluid type in the main cycle, while the performances of the cooling water circulation pumps are so low and can be neglected.
- The friction losses are negligible.

2.3. Energy analysis

Considering steady state condition and ignoring the kinetic and potential energies variations, the energy balance for a system component as a control volume can be written as:

$$\dot{Q} - \dot{W} = \sum_e \dot{m}_e h_e - \sum_i \dot{m}_i h_i \quad (1)$$

where $\dot{Q}$, $\dot{W}$ and h represents heat transfer rate, power and specific enthalpy, respectively. Equation (1) expresses that the total rate of energy entering the control volume equals the total rate of energy leaving it. The equations applied to calculate the first law efficiency of the PTORC and STORC systems are provided in Table 2.

2.4. Exergy analysis

Exergy is defined as the maximum work achieved by the combination of a system and its environment, as the system transmits from a certain state to the dead state while interacting heat with the environment only. The exergy flow rate of a stream at a specified state is written as:

$$\dot{E}_i = \dot{m}_i((h_i - h_0) - T_0(s_i - s_0)) \quad (2)$$

In Equation (2), the subscript 0 symbolizes the value of a thermodynamic property at the dead state.

The exergy rate balance for a system component as a control volume can be expressed as:

$$\sum \dot{E}x_i + \sum \dot{Q}_i \left(1 - \frac{T_0}{T_i}\right) = \dot{W}_{cv} + \sum \dot{E}x_e + \dot{E}x_{Loss} + \dot{E}x_D \quad (3)$$

where $\sum \dot{E}x_i$ and $\sum \dot{E}x_e$ denote the total rate of exergy entering the control volume and exiting it, respectively. Also, $\dot{E}x_{Loss}$ and $\dot{E}x_D$ indicates the exergy loss and exergy destruction during the process. Furthermore $\sum \dot{Q}_i(1 - T_0/T_i)$ and $\dot{W}_{cv}$ show exergy transferring, by heat transfer and work, respectively. The exergy balance for each component of the STORC and PTORC systems are presented in Table 3.

Table 1
The working fluids properties [13].

Fluid	Composition		Chemical formula	Critical temperature (°C)	Critical pressure (kPa)	Safety group	ODP	GWP	Type of the fluid
R402A	R125/290/22	(60/2/38)	$CHF_2CF_3/CH_3CH_2CH_3/CHC_1F_2$	75.5	4181	A1	0.019	2330	Wet
R404A	R125/143a/134a	(44/52/4)	$CHF_2CF_3/CH_3CF_3/CH_2FCF_3$	72.1	3651	A1	0	3260	Isentropic
R407A	R32/125/134a	(20/40/40)	$CH_2F_2/CHF_2CF_3/CH_2FCF_3$	82.8	4480	A1	0	1770	Wet
R410A	R32/125	(50/50)	CH_2F_2/CHF_2CF_3	71.4	4801	A1	0	1730	Wet
R422A	R125/134a/600a	(85.1/11.5/3.4)	$CHF_2CF_3/CH_2FCF_3/(CH_3)_3CH$	71.73	3749	A1	0	3040	Isentropic
R438A	R125/134a/32/600/601a	(45/44.2/8.5/1.7/0.6)	$CHF_2CF_3/CH_2FCF_3/CH_2F_2/C_4H_{10}/C_5H_{12}$	85.5	4096	A1	0	2265	Isentropic
R402B	R125/290/22	(38/2/60)	$CHF_2CF_3/CH_3CH_2CH_3/CHC_1F_2$	82.6	4402	A1	0.03	2080	Wet
R403B	R290/22/218	(5/56/39)	$CH_3CH_2CH_3/CHC_1F_2/C_3F_8$	90	3807	A1	0.028	3680	Wet
R422D	R125/134a/600a	(65.1/31.5/3.4)	$CHF_2CF_3/CH_2FCF_3/(CH_3)_3CH$	79.58	3749	A1	0	2620	Isentropic
R22M	R125/134a/600a	(46.6/50.0/3.4)	$CHF_2CF_3/CH_2FCF_3/(CH_3)_3CH$	89.9	3840	A1	0	1950	Isentropic
R245fa	Pure	Fluid	$C_3H_3F_5$	154.1		B1	0	1030	Dry

Table 2
Governing equations applied to energy analysis of the PTORC and STORC.

Components	PTORC	STORC
Turbine	$\dot{W}_t = \dot{m}_{wf,1}(h_3 - h_4) + \dot{m}_{wf,2}(h_6 - h_4)$	$\dot{W}_t = \dot{m}_{wf,1}(h_5 - h_7) + \dot{m}_{wf,2}(h_6 - h_7)$
Evaporator 1	$\dot{Q}_{e1} = \dot{m}_{wf,1}(h_3 - h_2)$	$\dot{Q}_{e1} = \dot{m}_{wf,1}(h_5 - h_4)$
Evaporator 2	$\dot{Q}_{e2} = \dot{m}_{wf,2}(h_5 - h_6)$	$\dot{Q}_{e2} = \dot{m}_{wf,1}(h_3 - h_2) + \dot{m}_{wf,2}(h_6 - h_3)$
Condenser	$\dot{Q}_c = (\dot{m}_{wf,1} + \dot{m}_{wf,2})(h_4 - h_1)$	$\dot{Q}_c = (\dot{m}_{wf,1} + \dot{m}_{wf,2})(h_7 - h_1)$
Pump 1	$\dot{W}_{p1} = \dot{m}_{wf,1}(h_5 - h_1)$	$\dot{W}_{p1} = (\dot{m}_{wf,1} + \dot{m}_{wf,2})(h_2 - h_1)$
Pump 2	$\dot{W}_{p2} = \dot{m}_{wf,2}(h_2 - h_1)$	$\dot{W}_{p2} = \dot{m}_{wf,1}(h_4 - h_3)$
Overall System	$\dot{W}_{net} = \eta_m \eta_g \dot{W}_t - \dot{W}_{p1} - \dot{W}_{p2}$	$\dot{W}_{net} = \eta_m \eta_g \dot{W}_t - \dot{W}_{p1} - \dot{W}_{p2}$
	$\eta_{en} = \dot{W}_{net}/(\dot{Q}_{e1} + \dot{Q}_{e2})$	$\eta_{en} = \dot{W}_{net}/(\dot{Q}_{e1} + \dot{Q}_{e2})$

Table 3
Formulation of exergy balance for PTORC and STORC components.

Components	PTORC	STORC
Turbine	$\dot{E}x_{D,t} = T_0(\dot{m}_{wf,1}(s_4 - s_3) + \dot{m}_{wf,2}(s_4 - s_6))$	$\dot{E}x_{D,t} = T_0(\dot{m}_{wf,1}(s_7 - s_5) + \dot{m}_{wf,2}(s_7 - s_6))$
Evaporator 1	$\dot{E}x_{D,e1} = T_0[\dot{m}_{wf,1}(s_3 - s_2) - \dot{m}_{gf}(s_8 - s_7)]$	$\dot{E}x_{D,e1} = T_0[\dot{m}_{wf,1}(s_5 - s_4) - \dot{m}_{gf}(s_9 - s_8)]$
Evaporator 2	$\dot{E}x_{D,e2} = T_0[\dot{m}_{wf,2}(s_6 - s_5) - \dot{m}_{gf}(s_9 - s_8)]$	$\dot{E}x_{D,e2} = T_0[\dot{m}_{wf,2}(s_6 - s_2) - \dot{m}_{gf}(s_{10} - s_9)]$
Condenser	$\dot{E}x_{D,cond} = T_0[(\dot{m}_{wf,1} + \dot{m}_{wf,2})(s_4 - s_1) - \dot{m}_{cw}(s_{11} - s_{10})]$	$\dot{E}x_{D,cond} = T_0[(\dot{m}_{wf,1} + \dot{m}_{wf,2})(s_7 - s_1) - \dot{m}_{cw}(s_{12} - s_{11})]$
Pump 1	$\dot{E}x_{D,p1} = \dot{m}_{wf,1}T_0(s_5 - s_1)$	$\dot{E}x_{D,p1} = (\dot{m}_{wf,1} + \dot{m}_{wf,2})T_0(s_2 - s_1)$
Pump 2	$\dot{E}x_{D,p2} = \dot{m}_{wf,2}T_0(s_2 - s_1)$	$\dot{E}x_{D,p2} = \dot{m}_{wf,1}T_0(s_4 - s_3)$
Overall system	$\dot{E}x_{D,total} = \dot{E}x_{D,t} + \dot{E}x_{D,e1} + \dot{E}x_{D,e2} + \dot{E}x_{D,cond} + \dot{E}x_{D,p1} + \dot{E}x_{D,p2}$	$\dot{E}x_{D,total} = \dot{E}x_{D,t} + \dot{E}x_{D,e1} + \dot{E}x_{D,e2} + \dot{E}x_{D,cond} + \dot{E}x_{D,p1} + \dot{E}x_{D,p2}$
	$\epsilon_{ex} = \dot{W}_{net}/\dot{E}x_{gw}$	$\epsilon_{ex} = \dot{W}_{net}/\dot{E}x_{gw}$

3. Validation

Using the data reported by Li et al. [22] for PTORC and STORC, with the same heat source and heat sink and having R245fa as the working fluid, the present work is validated as shown in Table 4. The maximum relative mean square of the errors (E_{rms}) is 7.18%, which is calculated for the mass flow rate of the working fluid in the low pressure evaporator of the PTORC. Moreover, as it is obvious in Table 4, the minimum relative mean square of the errors is only 0.7%, which belongs to IGWT (intermediate geothermal water temperature), demonstrating that the numerical calculation of the present model is reliable.

4. Optimization

4.1. Multi-objective optimization

Engineering problems sometimes encounter several incompatible targets that must be contended simultaneously. In such cases, a multi-objective optimization based on an evolutionary algorithm is a suitable and commodious procedure to assign the optimal solution and optimum design parameters for the system.

4.2. Genetic algorithm

Genetic algorithm, which was first presented by Holland [23], applies an iterative method to find an optimal solution and emulates the principles of biological evolutionary processes [24]. In the genetic algorithm, random numerous individuals are created as a primitive generation. In each population, the individuals are chosen based on their compatibility with respect to the objective functions. Usually the members with high conformity to objective functions are selected in order to reproduce a new generation. There are two significant operators in the genetic algorithm optimization method: cross over and mutation. The cross over operator compounds chromosomes as parents in order to produce new chromosomes called offspring. Because chromosomes with higher opportuneness are chosen as parents frequently, it is expected that the new generation would have a higher fitness with respect to the targets. Thus, the cross over operator leads the process to be converged. But, the mutation operator causes variations chaotically in chromosomes features and makes the optimization process away from the local optimum [25,26]. The flow chart of the genetic algorithm applied here, is shown in Fig. 4. In the present study to obtain an optimized solution, MATLAB software optimization toolbox using genetic algorithm is applied. The tuning parameters used for the genetic algorithm optimization in the present work are given in Table 5.

4.3. Objective functions

For multi-objective optimization aim of the proposed system,

Table 4
Validation of the results obtained from the present work with data reported by Tailu Li et al. [22].

$T_{gw,in}$ (°C)	$\dot{m}_{wf}$ (kg/s)				T_{eva} (°C)				$IGWT$ (°C)		P_{cond} (Mpa)
	PTORC		STORC		PTORC		STORC		PTORC	STORC	
	High	Low	High	Low	High	Low	High	Low			
90											
Li et al. [22]	14.21	11.96	13.66	12.28	77	67	77	70	79	82	0.1772
Present work	14.486	11.301	14.47	11.18	77	67	77	70	78.675	81.4	0.1772
95											
Li et al. [22]	16.62	14.62	18.26	14.1	80	68	80	71	81	84	0.1772
Present work	18.39	12.700	18.38	14.07	80	68	80	71	80.498	84.16	0.1772
100											
Li et al. [22]	24.23	15.64	20.50	17.79	82	67	84	73	82	88	0.1772
Present work	24.17	14.813	20.65	17.05	82	67	84	73	80.835	87.83	0.1772
105											
Li et al. [22]	26.51	18.56	24.76	19.67	86	68	87	74	84	90	0.1772
Present work	26.61	17.851	24.83	19.67	86	68	87	74	83.664	90.34	0.1772
110											
Li et al. [22]	32.67	18.56	26.79	23.49	88	68	91	76	84	94	0.1772
Present work	32.704	17.753	27.38	22.45	88	68	91	76	83.645	93.8	0.1772
115											
Li et al. [22]	38.78	18.56	30.62	25.56	90	68	95	78	84	97	0.1772
Present work	38.95	17.365	30.09	25.14	90	68	95	78	83.449	97.33	0.1772
120											
Li et al. [22]	42.13	20.96	36.28	25.83	94	69	97	80	86	99	0.1772
Present work	41.93	19.391	36.6	24.34	94	69	97	80	85.683	98.7	0.1772
Errors	$E_{rms} = 4.09\%$	$E_{rms} = 7.18\%$	$E_{rms} = 2.52\%$	$E_{rms} = 4.65\%$					$E_{rms} = 0.7\%$	$E_{rms} = 0.37\%$	

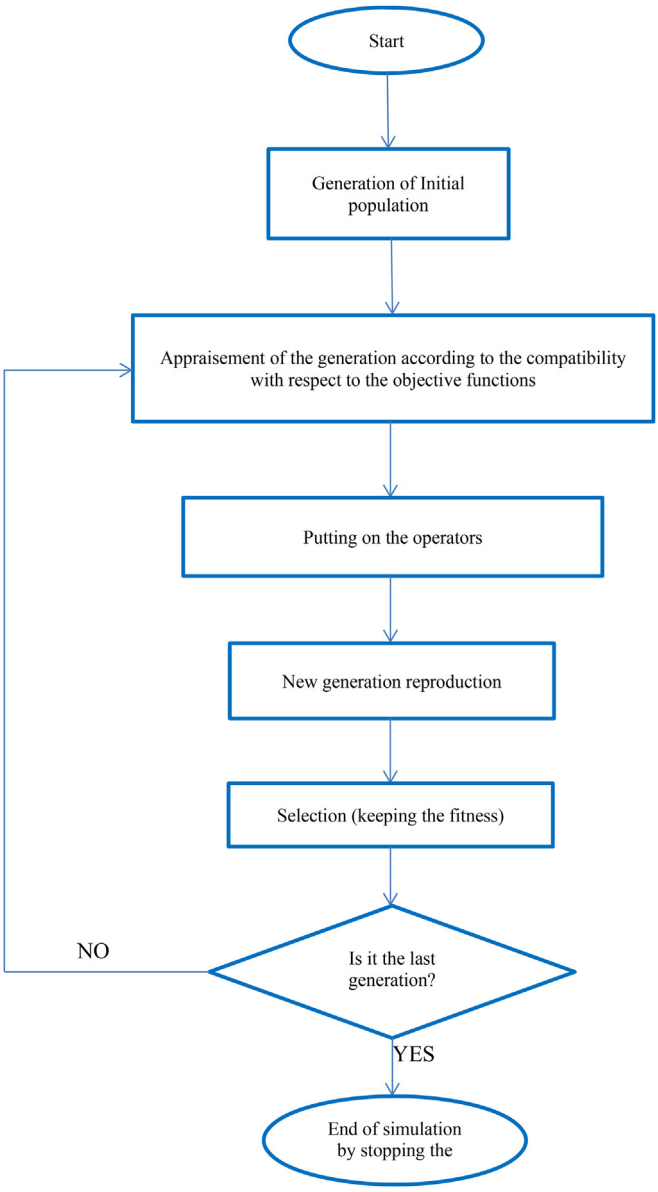

Fig. 4. Genetic algorithm flow chart.

Table 5
Tuning parameters in the genetic algorithm optimization program.

Tuning parameters	Value
Population size	500
Maximum number of generation	600
Probability of crossover	85%
Probability of mutation	1%
Selection process	Tournament
Tournament size	2

two momentous parameters including the net power output (to be maximized) and TSP (turbine size parameter) (to be minimized) are considered as objective functions. The net power output and TSP for the system are defined as follows:

Net power output (objective function I)

$$\dot{W}_{net} = \eta_m \eta_g \dot{W}_t - \dot{W}_{p1} - \dot{W}_{p2} \quad (4)$$

TSP (turbine size parameter) (objective function II)

$$TSP = \frac{\sqrt[2]{\dot{m}_{wf} v_{out,is}}}{\sqrt[4]{h_{in} - h_{out,is}}} \quad (5)$$

4.4. Decision variables and constraints

In the present study decision variables are considered as following: the first evaporator pressure (P_{e1}), the second evaporator pressure (P_{e2}), the pinch point temperature difference in evaporator 1 (ΔT_{PP}) and the superheating degree in evaporator 1 (ΔT_{sup}). Ranges of the design parameters and constraints are given in Table 6.

5. Results and discussion

5.1. Configuration analysis

In this section, the performance of three various configurations, including subcritical simple ORC, PTORC and STORC with different working fluids, from the viewpoint of the first and second laws of thermodynamics are investigated and compared. Table 7 shows the system parameters which are considered in this study.

The results of this comparison are presented in Table 8. In all cases, the maximum pressure of the cycle is assumed to be 90% of working fluid critical pressure.

According to Table 8, it can be concluded that the simple ORC has the lowest amount of the net power output ($\dot{W}_{net}$) and STORC has the highest one. This is because; for the same thermodynamic condition at the inlet and outlet of the turbine in all three configurations, the total mass flow rate in turbine for simple ORC is lower than STORC and PTORC. Therefore, based on equations mentioned in Table 2, the net power output for simple ORC will be less than the other configurations. Moreover, as can be seen in Table 8, in all of configurations, more net power output is achieved by using zeotropic working fluids than that of the pure fluids. So that, using zeotropic mixtures instead of a pure fluid such as R245fa results in 27.76%, 24.98% and 24.79% improvement of the net power output in the simple ORC, PTORC and STORC systems, respectively.

By a close look at Table 8, it is evident that the mass flow rate of the evaporator 2 in STORC is more than PTORC which leads to higher net power output generation in STORC. This is because of; in STORC system, the refrigerant enters the evaporator 1 with higher pressure in comparison to PTORC (Working fluid pressure at the inlet of the evaporator 1 for STORC equals to the evaporator 2 pressure and for PTORC equals to the condenser pressure). So in STORC case study, the working fluid enthalpy at the inlet of the evaporator 1 is higher than the PTORC; Due to this reason the temperature of the geothermal water at the outlet of the evaporator 1 for STORC is higher than PTORC. Thus the thermal reservoir enters the second evaporator with higher enthalpy. Therefore, in evaporator 2 of STORC, more energy can be achieved from geothermal water and because of this matter secondary mass flow rate ($\dot{m}_{wf2}$) increases.

According to the Equation (5), and considering the same thermodynamic conditions for all three configurations at the inlet and outlet of the turbine, it can be concluded that TSP has similar trend with the total mass flow rate. Also, as can be concluded from Table 8, in all of configurations, using zeotropic mixtures instead of a pure fluid leads to lower amounts of TSP.

Referring to Table 8, it can be observed that STORC and PTORC outlet geothermal temperatures (T_{GW}) are less than that of the simple ORC. Because of; these two configurations absorb more

Table 6
List of constraints and ranges of design parameters for system optimization.

Constraints and decision variables ranges	Reason
$T_{cond} = 25\ ^{\circ}C$	Cooling water temperature limitation
$0.67 < P_{e1}/P_c < 0.91$	For driving the evaporator 1 efficiently
$0.4 < P_{e2}/P_c < 0.6$	For driving the evaporator 2 efficiently
$4 < \Delta T_{PP} < 9$	Geothermal water heat supply limitation
$5 < \Delta T_{sup} < 15$	Commercial availability

Table 7
The system parameters used in the present study.

Geothermal water mass flow rate (kg/s)	50
Geothermal water temperature (°C)	100
Turbine isentropic efficiency (%)	80
Pumps isentropic efficiency (%)	70
Mechanical efficiency (%)	97
Generator efficiency (%)	98

exergy gained by the thermal reservoir for PTORC is more than the simple ORC. Therefore, according to the definition of the exergy efficiency presented in Table 3, the amount of ε_{ex} for PTORC is obtained less than the simple ORC. On the other hand, the highest value of the exergy efficiency could be achieved by the STORC system.

Also, the exergy loss ($\dot{E}x_{loss}$) shows the same behavior as the

Table 8
Comparison of the three various configurations for ORC from the energy and exergy point of view.

ORC	$\dot{W}_{net}$(kW)	η_{en} (%)	ε_{ex} (%)	TSP(m)	T_{GW} (°C)	$\dot{m}_{wf}$(kg/s)	$\dot{E}x_D$ (kW)	$\dot{E}x_{loss}$(kW)	$\dot{E}x_D + \dot{E}x_{loss}$(kW)	
R22M	643.60	8.75	50.06	0.076	64.81	41.30	609.01	604.82	1213.83	
R402A	757.83	7.52	47.37	0.083	51.80	65.65	803.10	290.75	1093.85	
R402B	645.49	8.43	48.73	0.071	63.38	45.18	645.95	565.92	1211.86	
R403B	745.38	7.32	46.31	0.088	51.32	67.83	826.0	280.95	1106.95	
R404A	774.59	6.98	45.78	0.091	46.95	69.09	877.86	198.42	1076.28	
R407A	700.14	8.71	51.01	0.071	61.57	41.47	636.48	517.93	1154.41	
R410A	741.93	7.02	45.09	0.073	49.48	54.39	865.74	244.87	1110.61	
R422A	807.59	6.78	45.87	0.097	43.20	82.75	911.69	136.74	1048.42	
R422D	770.21	7.90	49.06	0.087	53.55	59.99	760.18	327.42	1087.60	
R438A	678.08	8.74	50.71	0.074	62.91	41.62	624.22	553.38	1177.60	
R245fa	542.90	9.19	50.28	0.14	71.76	24.81	508.81	810.86	1319.68	
PTORC	$\dot{W}_{net}$(kW)	η_{en} (%)	ε_{ex} (%)	TSP(m)	T_{GW} (°C)	$\dot{m}_{wf1}$(kg/s)	$\dot{m}_{wf2}$(kg/s)	$\dot{E}x_D$(kW)	$\dot{E}x_{loss}$(kW)	$\dot{E}x_D + \dot{E}x_{loss}$(kW)
R22M	833.97	6.97	47.25	0.0978	42.90	41.68	26.89	888.53	132.12	1020.66
R402A	825.05	6.27	44.81	0.0962	37.22	66.05	20.88	974.05	56.08	1030.13
R402B	798.10	6.42	44.40	0.092	40.67	45.54	29.56	958.60	99.84	1058.4
R403B	802.69	5.91	43.09	0.102	35.23	68.21	23.69	1019.45	34.25	1053.69
R404A	813.08	5.98	43.62	0.101	35.14	69.45	16.17	1009.37	33.39	1042.76
R407A	872.19	7.03	48.57	0.089	40.78	41.80	23.52	879.09	101.39	980.49
R410A	784.93	5.75	42.05	0.083	34.88	54.67	16.61	1041.67	30.70	1072.38
R422A	833.07	6.03	44.44	0.105	34.08	82.75	14.07	998.92	22.82	1021.74
R422D	858.03	6.73	47.23	0.1004	39.22	59.99	19.49	914.86	80.55	995.41
R438A	861.05	7.02	48.20	0.094	41.46	41.97	25.22	881.27	110.94	992.21
R245fa	697.84	8.49	49.94	0.16	60.88	25.00	9.8	663.53	500.10	1163.63
STORC	$\dot{W}_{net}$(kW)	η_{en} (%)	ε_{ex} (%)	TSP(m)	T_{GW} (°C)	$\dot{m}_{wf1}$(kg/s)	$\dot{m}_{wf2}$(kg/s)	$\dot{E}x_D$ (kW)	$\dot{E}x_{loss}$(kW)	$\dot{E}x_D + \dot{E}x_{loss}$(kW)
R22M	908.73	8.55	54.91	0.0993	49.35	41.68	28.95	778.39	242.45	1020.8
R402A	866.24	7.43	49.75	0.0966	44.44	66.05	21.57	885.55	156.12	1041.6
R402B	859.02	7.83	50.99	0.0921	47.74	45.54	29.77	841.9	212.63	1054.5
R403B	845.41	7.01	47.74	0.1021	42.53	68.21	23.92	924.72	126.61	1051.3
R404A	843.83	6.98	47.58	0.1014	42.35	69.45	16.19	933.0	123.85	1056.8
R407A	940.30	8.53	55.63	0.0903	47.44	41.80	25.18	767.33	207.23	974.57
R410A	817.65	6.72	45.98	0.0838	42.03	54.66	17.13	954.94	119.24	1074.1
R422A	857.59	6.97	47.96	0.1059	42.22	82.74	15.03	931.49	109.22	1040.7
R422D	913.99	8.06	53.25	0.1024	45.93	59.99	22.73	825.72	180.89	1006.6
R438A	933.79	8.56	55.58	0.0957	48.01	41.97	27.15	768.78	217.44	986.23
R245fa	753.66	8.85	52.54	0.21	59.40	25.00	19.18	888.85	462.88	1351.74

energy from geothermal water. Moreover, as a comparison between STORC and PTORC, it can be seen that the PTORC has the lowest amount of T_{GW}. This is because of; as mentioned above, the geothermal water temperature at the inlet of the second evaporator for PTORC is less than STORC.

Another point that can be concluded from Table 8, is that the PTORC has the minimum exergy efficiency (ε_{ex}) among the three different configurations. It can be justified because, however the net power output for PTORC is more than the simple ORC, but

outlet geothermal temperature, because the exergy loss depends on this temperature. As mentioned before, the main source of the exergy destruction is evaporator because of the temperature mismatching between the source and the working fluid. This temperature mismatching for STORC is lower than PTORC, leading to reduction of the exergy destruction ($\dot{E}x_D$). On the other hand simple ORC has the minimum exergy destruction. This is because of; however temperature mismatching in simple ORC is more than PTORC and STORC, but it should be noticed that the same maximum

pressure for all configurations are considered. This means, In fact for mentioned thermodynamic conditions, STORC and PTORC act as simple ORC with extra components which leads to increasing the exergy destruction. Finally, the last column in Table 8 ($\dot{E}x_D + \dot{E}x_{loss}$), denotes sum of the exergy destruction in the system ($\dot{E}x_D$) and the exergy loss ($\dot{E}x_{loss}$).

In the present study the geothermal water is considered as an energy source, which has two significant characteristics: by using this kind of source, there is no need for fuel consumption and this source is always easily available. With attention to these specifications, the net power output is more important than the efficiency. The results of this section indicates that using STORC configuration could yield to higher values of the net power output ($\dot{W}_{net}$) comparing to the other configurations for all working fluids. Therefore, in this work STORC is selected as the most suitable configuration.

5.2. Parametric study

In this section for STORC configuration, the influence of the evaporator 1 pressure (P_{e1}/P_c), the evaporator 2 pressure (P_{e2}/P_c), the pinch point temperature difference (ΔT_{PP}) and the superheating degree (ΔT_{sup}) are investigated on the net power output ($\dot{W}_{net}$) and the TSP (turbine size parameter).

Fig. 5 shows variation of the net power output with increase of the evaporator 1 pressure. As can be seen in this figure, by increasing the evaporator 1 pressure, for many of the working fluids the net power output increases continuously and for some of them an optimum point is achieved. This is justified because, by considering that the lower pressure of the cycle during this variation mains constant, increasing P_{e1} has two conflicting effects on the cycle: the first is increasing the turbine pressure difference leading to more power generation in the turbine and the second one is decreasing the mass flow rate which has a negative effect on power generation. It is observed that for many of the working fluids the first effect overcomes the second one which causes increasing the power.

Fig. 6 outlines the effect of the evaporator 2 pressure on the net power output. This figure shows that there is a maximum amount of the net power output by changing P_{e2} for all of the working fluids. Same as P_{e1}, increasing P_{e2} has two conflicting influences on the system performance: the first one is increasing of the working fluid enthalpy at the inlet of the turbine that has a positive effect on the power generation and the second effect is evaporator 2 mass flow rate ($\dot{m}_{wf2}$) reduction leading to decreasing of the power generation. In all of the working fluids for lower pressure levels of the evaporator 2, by increasing P_{e2} the net power output increases because the dominant effect is the first one. This behavior changes from a particular amount of P_{e2} for each working fluid. This is because of; at the higher pressure levels of evaporator 2 the second effect overcomes the first one.

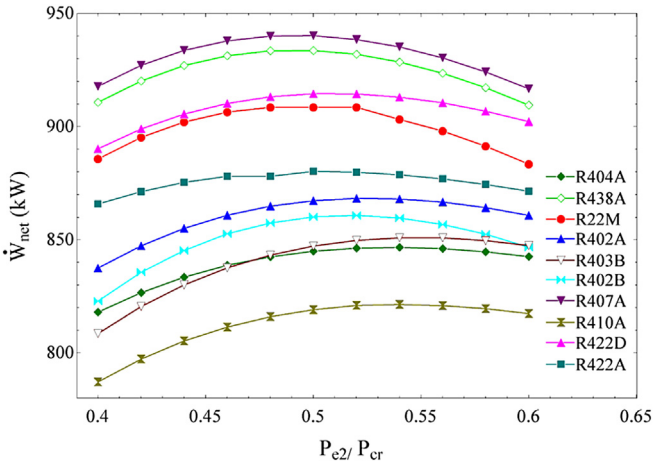

Fig. 6. Variation in the net power output with the evaporator 2 pressure.

The effect of the pinch point temperature difference (ΔT_{PP}) on the variation of the net power output is depicted in Fig. 7. From this figure it is obvious that by increasing ΔT_{PP}, the net power output reduces continuously. This is because of; as ΔT_{PP} increases, energy gained by the thermal reservoir decreases and because of this reason the total mass flow rate of the cycle decreases which leads to reduction of the net power output.

Fig. 8 illustrates the influence of the superheating degree (ΔT_{sup}) increasing, on the net power output. Referring to this figure ΔT_{sup} has no significant effect on $\dot{W}_{net}$. Because when ΔT_{sup} increases, turbine inlet enthalpy increases but on the other hand, total mass flow rate decreases. Consequence of these mentioned effects leads to no considerable change in the net power output.

The influence of the evaporator 1 pressure (P_{e1}) on the TSP (turbine size parameter) is presented in Fig. 9. As can be seen, rising of P_{e1} leads to reduction of TSP. According to Equation (5), turbine size parameter depends on the mass flow rate and the turbine

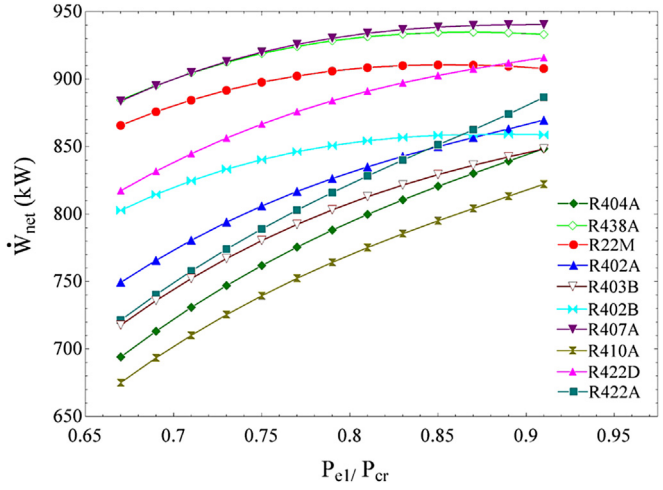

Fig. 5. Variation in the net power output with the evaporator 1 pressure.

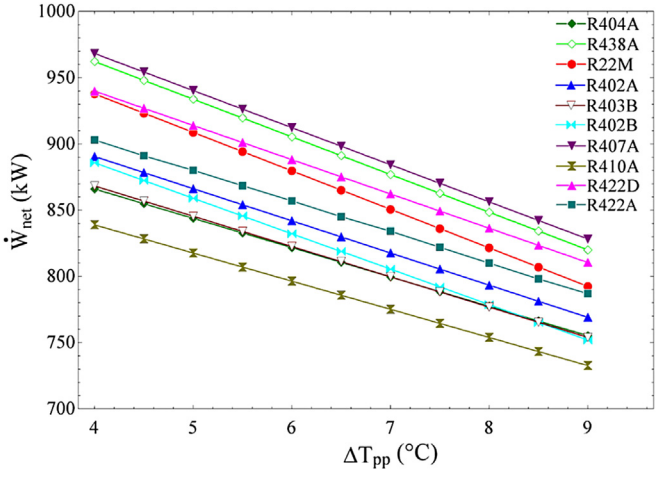

Fig. 7. Variation in the net power output with the pinch point temperature difference.

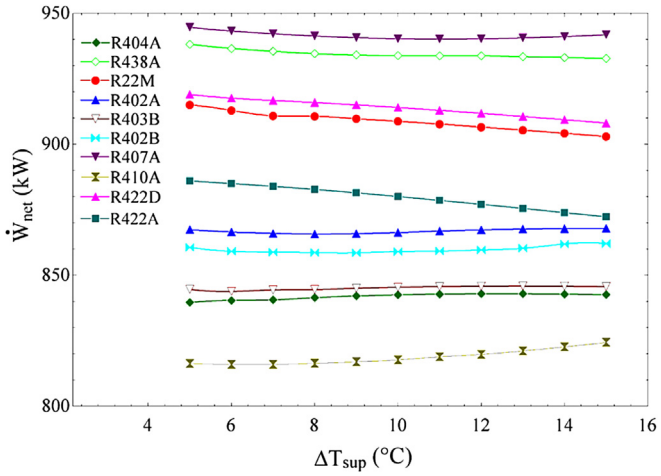

Fig. 8. Variation in the net power output with the superheating degree.

outlet specific volume directly and inversely depends on the turbine inlet and isentropic outlet enthalpy difference. As discussed above, by raising the evaporator 1 pressure, the total mass flow rate decreases and turbine inlet enthalpy increases. These two mentioned impacts leads to reduction of TSP.

Variation of TSP by increasing the evaporator 2 pressure (P_{e2}) is demonstrated in Fig. 10. Referring to this figure, it is evident that for all of the working fluids, TSP reduces by increasing the P_{e2}. The reason of this behavior is that when P_{e2} raises, the total mass flow rate decreases which leads to decline of TSP.

Fig. 11 represents the effect of the pinch point temperature difference (ΔT_{PP}) on TSP. It can be concluded from this figure that TSP reduces by increase of the ΔT_{PP}. Because as the Pinch point temperature difference increases, the total mass flow rate reduces. Therefore, the consequence of ΔT_{PP} rising is TSP declining.

Fig. 12 shows the change in TSP value by increasing the superheating degree (ΔT_{sup}). As it is obvious, increasing the ΔT_{sup} leads to TSP reduction. When ΔT_{sup} raises, the total mass flow rate declines and turbine inlet enthalpy grows. These mentioned trends result in reduction of TSP for all of the working fluids.

A close look at Figs. 5–8 which show the variation of the net power output by varying the design parameters including P_{e1}, P_{e2}, ΔT_{PP} and ΔT_{sup}, it can be concluded that R407A has the best performance from the viewpoint of the power production, among all

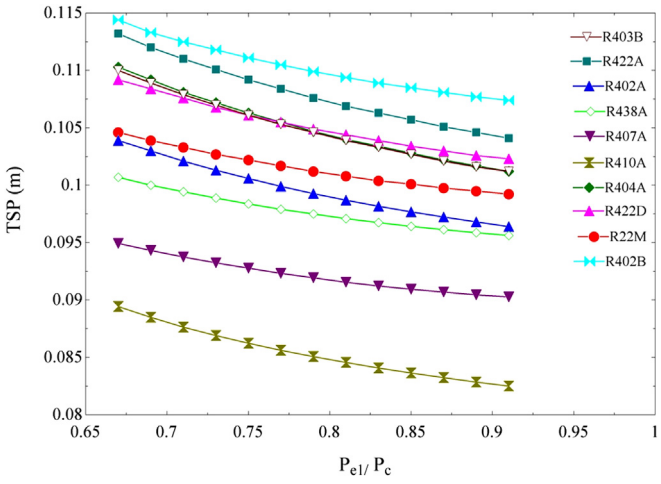

Fig. 9. Variation in TSP with the evaporator 1 pressure.

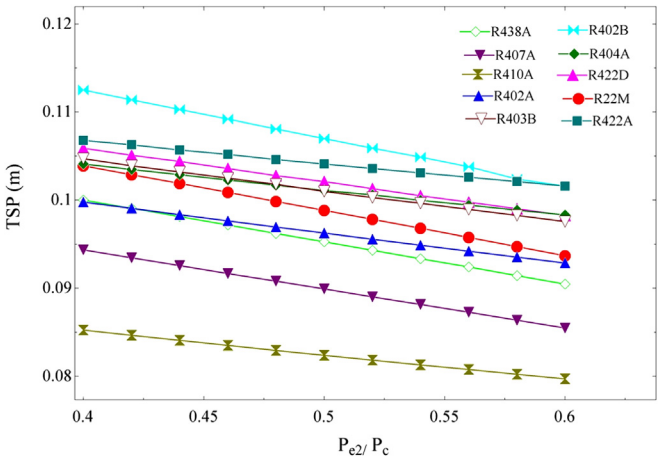

Fig. 10. Variation in TSP with the evaporator 2 pressure.

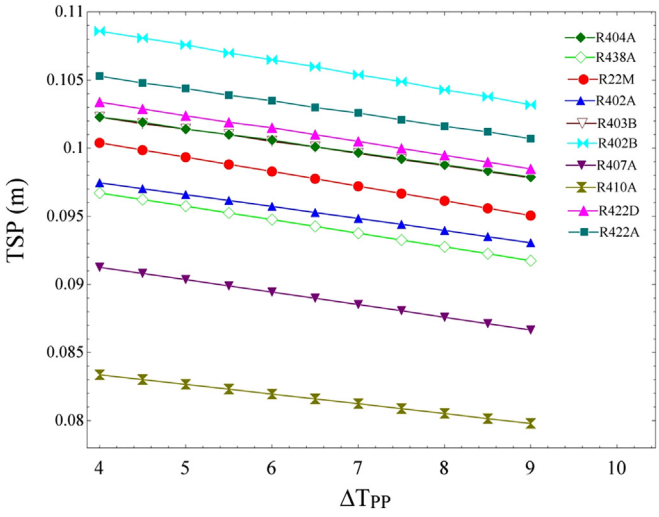

Fig. 11. Variation in TSP with the pinch point temperature difference.

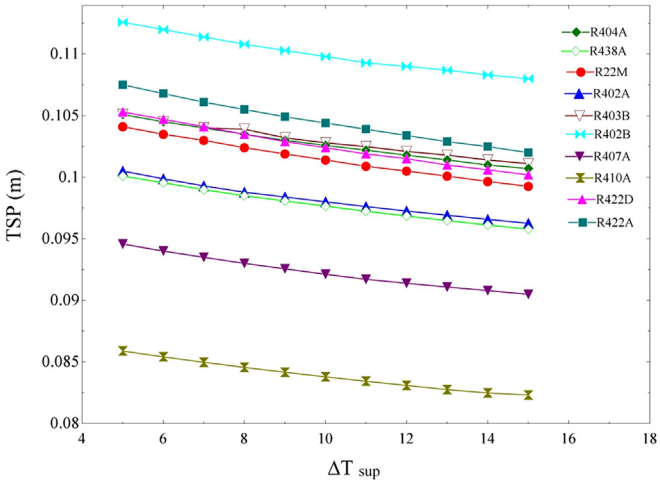

Fig. 12. Variation in TSP with the superheating degree.

working fluids. On the other hand, reviewing Figs. 9–12 which illustrate changing TSP with decision variables, reveal that R410A has the minimum amount of TSP, and the second lowest value of

TSP belongs to R407A. Therefore, it can be deduced that STORC system running by R407A as a working fluid, has the maximum value of power production and second minimum amount of TSP. Finally; with respect to the objective functions, R407A could be introduced as the most suitable working fluid for STORC configuration.

5.3. Optimization results

In this section, the results of the multi-objective optimization including the Pareto optimal frontier for STORC system with R407A as the selected working fluid are presented in Fig. 13. The objective functions as expressed in Equations (4) and (5), are the net power output and TSP.

Referring to Fig. 13, the maximum value of the net power output occurs at design point A (967.7 kW), where TSP has its highest value (0.08946 m). Moreover, the minimum amount of the net power output is achieved at design point B (810.7 kW), while TSP is the lowest (0.07962 m).

Therefore, the design point A is selected as the final optimum point when the net power output is considered as the only objective function, and the design point B is chosen as the final optimum point if TSP is considered as a sole objective function.

In the multi-objective optimization method, each point introduced by the Pareto frontier solution, can be elected as an optimum point. Thus, according to the emphasis of the objective functions, the final optimal point is determined by the decision maker.

In the present work, in order to identify the final optimal point, the equilibrium point is defined as a first step. The equilibrium point is a hypothetical point which on that, both objective functions obtain their optimal values simultaneously, independent of each other.

A point on the Pareto frontier which has the minimum distance from the equilibrium point is identified as the final optimal point [27]. The decision-making process using the mentioned approach is depicted in Fig. 13. Values of the objective functions including the net power output and TSP at the final optimal point are achieved 877 kW and 0.08218 m, respectively. Also, the values of the design parameters and performance characteristics for STORC system at this point are given in Table 9.

Fig. 14 shows the Grassmann diagrams of the STORC system at the optimum condition. Referring to Fig. 14a, it is indicated that by considering the evaporator 1 and evaporator 2 as a single evaporation component, the maximum exergy destruction belongs to this component. This is because of; however using the zeotropic mixtures as the working fluid and applying two stage evaporator configuration lead to the exeregy destruction reduction in the evaporators, nevertheless due to the temperature difference between the thermal source and the working fluid, the highest amount of the exergy destruction occurs in the evaporators. Also, as it can be seen in Fig. 14b, nearly 12% of the total energy input to the system converts to the useful work in turbine.

6. Conclusion

Thermodynamic modeling and multi-objective optimization are performed for three different configurations of the organic Rankine cycle, including simple ORC, PTORC and STORC running by ten zeotropic mixtures and one pure refrigerant as the working fluid. The main conclusions that can be obtained from the present work are listed as follows:

- From the viewpoint of the power generation, using zeotropic mixtures as the working fluid instead of a pure fluid such as R245fa, in all three types of configurations, including simple ORC, PTORC and STORC, leads to 27.76%, 24.98% and 24.79% improvement respectively.

Table 9
The optimizations results of the parameters for STORC system.

P_{e1}/P_c	0.90
P_{e2}/P_c	0.59
P_{e1} (kPa)	4032
P_{e2} (kPa)	2643.3
ΔT_{pp}	6.53
ΔT_{sup}	14.83
T_{cond} (°C)	25
$\dot{W}$(kW)	877
TSP (m)	0.08218
η_{en} (%)	9.79
ε_{ex} (%)	59.10
T_{GW} (°C)	57.35
$\dot{m}_{wf1}$ (kg/s)	34.90
$\dot{m}_{wf2}$ (kg/s)	19.57
$\dot{E}x_D$(kW)	663.52
$\dot{E}x_{loss}$(kW)	413.23
$\dot{E}x_D + \dot{E}x_{loss}$(kW)	1076.75

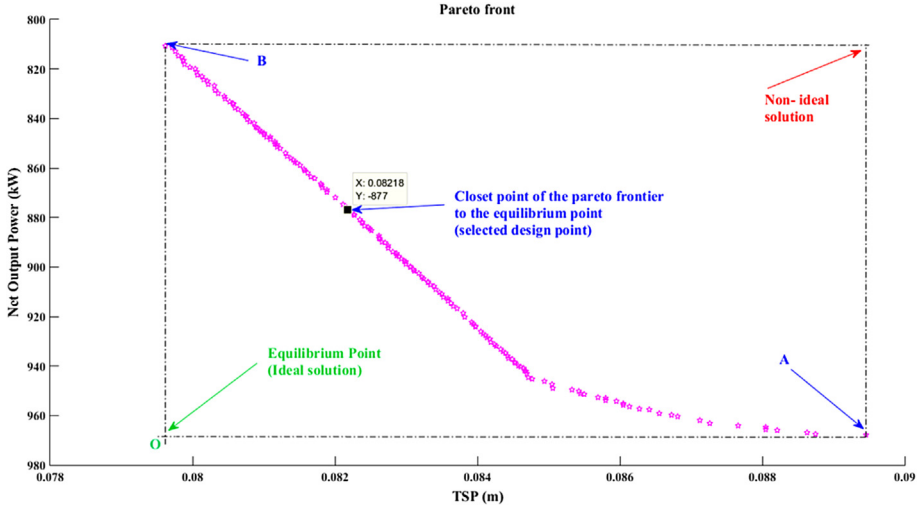

Fig. 13. Pareto optimal frontier attained by multi-objective optimization of the STORC system using R407A as the working fluid.

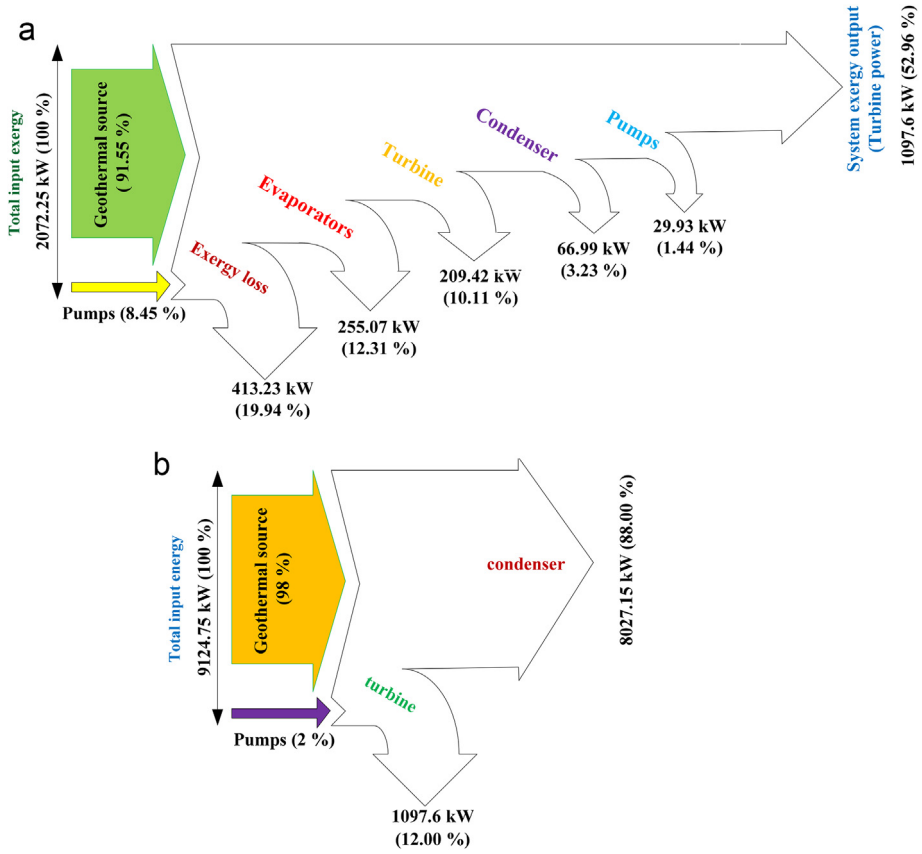

Fig. 14. a) Grassmann diagram (exergy flow diagram) of the STORC system for the optimal case. b) Grassmann diagram (energy flow diagram) of the STORC system for the optimal case.

- In all configurations using zeotropic mixtures leads to lower values of TSP, in comparison to a pure fluid.
- Considering the same thermodynamic conditions such as the condenser temperature and the maximum pressure of the cycle, for each working fluid, STORC represents better performance than the other configurations. As an example, for R407A, the net power output generated by STORC in comparison to PTORC and simple ORC is improved up to 7.81% and 34.3% respectively.
- Analysis results show that for the same thermodynamic conditions, using R407A in the STORC system, leads to the highest value of the net power output (940.30 kW) and the second lowest amount of TSP (0.0903 m).
- Considering the net power output generation and TSP as the two objective functions, it is observed that when the STORC system works at an evaporator 1 pressure, an evaporator 2 pressure, a pinch point temperature difference and a superheating degree of 0.9 P_c kPa, 0.59 P_c kPa, 6.53 °C and 14.83 °C respectively, the system takes on its optimal performance with the $\dot{W}_{net}$ and TSP values of 877 kW and 0.08218 m, respectively.
- The multi-objective optimization results demonstrate that an increase of 8.18% in the net power output generation is attained at the expenditure of just 3.21% increase in the TSP.
- At the final optimum design point of the STORC system using R407A as the working fluid, the values of the net power output and TSP are improved 24.76% and 57%, respectively, in comparison to the STORC running by R245fa as a pure fluid.

References

[1] U.S. Energy Information Administration. International energy outlook 2011. 2011. Washington, DC.
[2] Eurostat. Electricity prices for household consumers. 2013. http://www.epp.eurostat.ec.europa.eu.
[3] U.S. Energy Information Administration. Average retail price of electricity to ultimate customers. http://www.eia.gov.
[4] Bianchi M, De Pascale A. Bottoming cycles for electric energy generation: parametric investigation of available and innovative solutions for the exploitation of low and medium temperature heat sources. Appl Energy 2011;88(5):1500–9.
[5] Venkatarathnam G, Mokashi Girish, Srinivasa Murthy S. Occurrence of pinch points in condensers and evaporators for zeotropic refrigerant mixtures. Int J Refrig 1996;19(6):361–8.
[6] Kang Zhenhua, Zhu Jialing, Lu Xinli, Li Tailu, Wu Xiujie. Parametric optimization and performance analysis of zeotropic mixtures for an organic Rankine cycle driven by low-medium temperature geothermal fluids. Appl Therm Eng 2015;89:323–31.
[7] Radulovic Jovana, Beleno Castaneda Nadia I. On the potential of zeotropic mixtures in supercritical ORC powered by geothermal energy source. Energy Convers Manag 2014;88:365–71.
[8] Liu Bo-Tau, Chien Kuo-Hsiang, Wang Chi-Chuan. Effect of working fluids on organic Rankine cycle for waste heat recovery. Energy 2004;29(8):1207–17.
[9] Chen Yue, Han Dong, Pu Wenhao, He Weifeng. Thermal matching performance of a geothermal ORC system using zeotropic working fluids. Renew Energy 2015;80:746–54.
[10] Deethayat Thoranis, Kiatsiriroat Tanongkiat, Thawonngamyingsakul Chakkraphan. Performance analysis of an organic Rankine cycle with internal heat exchanger having zeotropic working fluid. Case Stud Therm Eng 2015;6:155–61.
[11] Lecompte Steven, Ameel Bernd, Ziviani Davide, Broek Martijn van den, Paepe Michel De. Exergy analysis of zeotropic mixtures as working fluids in Organic Rankine Cycles. Energy Convers Manag 2014;85:727–39.
[12] Li You-Rong, Du Mei-Tang, Wu Chun-Mei, Wu Shuang-Ying, Liu Chao. Potential of organic Rankine cycle using zeotropic mixtures as working fluids for waste heat recovery. Energy 2014;77:509–19.
[13] Habka Muhsen, Ajib Salman. Evaluation of mixtures performances in Organic Rankine Cycle when utilizing the geothermal water with and without cogeneration. Appl Energy 2015;154:567–76.
[14] Heberle Florian, Preißinger Markus, Brüggemann Dieter. Zeotropic mixtures as working fluids in Organic Rankine Cycles for low-enthalpy geothermal resources. Renew Energy 2012;37(1):364–70.
[15] Yari M. Performance analysis of the different organic Rankine cycles (ORCs)

using dry fluids. Int J Exergy 2009;6(3):323–42.
[16] Yari Mortaza. Exergetic analysis of various types of geothermal power plants. Renew Energy 2010;35(1):112–21.
[17] Ho Tony, Mao Samuel S, Greif Ralph. Increased power production through enhancements to the organic flash cycle (OFC). Energy 2012;45(1):686–95.
[18] Kanoglu Mehmet. Exergy analysis of a dual-level binary geothermal power plant. Geothermics 2002;31(6):709–24.
[19] Zhang HG, Wang EH, Fan BY. A performance analysis of a novel system of a dual loop bottoming organic Rankine cycle (ORC) with a light-duty diesel engine. Appl Energy 2013;102:1504–13.
[20] Yari M, Mehr AS, Zare V, Mahmoudi SMS, Rosen MA. Exergoeconomic comparison of TLC (trilateral Rankine cycle), ORC (organic Rankine cycle) and Kalina cycle using a low grade heat source. Energy 2015;83:712–22.
[21] Li Tailu, Zhu Jialing, Hu Kaiyong, Kang Zhenhua, Zhang Wei. Implementation of PDORC (parallel double-evaporator organic Rankine cycle) to enhance power output in oilfield. Energy 2014;68:680–7.
[22] Li Tailu, Zhang Zhigang, Lu Jian, Yang Junlan, Hu Yujie. Two-stage evaporation strategy to improve system performance for organic Rankine cycle. Appl Energy 2015;150:323–34.
[23] Holland John Henry. Adaptation in natural and artificial systems: an introductory analysis with applications to biology, control, and artificial intelligence. MIT Press; 1992.
[24] Srinivas Nidamarthi, Deb Kalyanmoy. Multiobjective optimization using nondominated sorting in genetic algorithms. Evol Comput 1994;2(3):221–48.
[25] Konak Abdullah, Coit David W, Smith Alice E. Multi-objective optimization using genetic algorithms: a tutorial. Reliab Eng Syst Saf 2006;91(9):992–1007.
[26] Sadeghi Mohsen, Mahmoudi SMS, Khoshbakhti Saray R. Exergoeconomic analysis and multi-objective optimization of an ejector refrigeration cycle powered by an internal combustion (HCCI) engine. Energy Convers Manag 2015;96:403–17.
[27] Sadeghi Mohsen, Chitsaz Ata, Mahmoudi SMS, Rosen Marc A. Thermoeconomic optimization using an evolutionary algorithm of a trigeneration system driven by a solid oxide fuel cell. Energy 2015;89:191–204.

Nomenclature

E: error
$\dot{E}x$: exergy rate (kW)
$\dot{E}x_D$: exergy destruction rate (kW)
$\dot{E}x_{loss}$: exergy loss rate (kW)
h: specific enthalpy (kJ/kg)
$\dot{m}$: mass flow rate (kg/s)
P: pressure (kPa)
T: temperature (°C)
$\dot{W}$: net power output (kW)

Acronyms

GWP: global warming potential
HRVG: heat recovery vapor generator
IGWT: intermediate geothermal water temperature
ODP: ozone depletion potential
ORC: organic Rankine cycle
PTORC: parallel two-stage evaporator organic Rankine cycle
STORC: series two-stage evaporator organic Rankine cycle
TSP: turbine size parameter

Subscripts

c: critical point
cond: condenser
cw: cooling water
e1: evaporator 1
e2: evaporator 2
en: energy
eva: evaporator
ex: exergy
gw: geothermal fluid
is: isentropic state
PP: pinch point
rms: relative mean square
sup: superheating
t: turbine
tot: total
wf: working fluid
wf1: mass flow rate of evaporator 1
wf2: mass flow rate of evaporator 2

Greek symbols

ϵ_{ex}: exergy efficiency
η_{en}: energy efficiency